7-1-2010

Viscosity Effects in Vibratory Mobilization of Residual Oil

Igor A. Beresnev

Wen Deng
Missouri University of Science and Technology, wendeng@mst.edu

Viscosity effects in vibratory mobilization of residual oil

Igor A. Beresnev[1] and Wen Deng[1]

ABSTRACT

The last decade has seen clarifications of the underlying capillary physics behind stimulation of oil production by seismic waves and vibrations. Computational studies have prevailed, however, and no viscous hydrodynamic theory of the phenomenon has been proposed. For a body of oil entrapped in a pore channel, viscosity effects are naturally incorporated through a model of two-phase core-annular flow. These effects are significant at the postmobilization stage, when the resistance of capillary forces is overcome and viscosity becomes the only force resisting an oil ganglion's motion. A viscous equation of motion follows, and computational fluid dynamics (CFD) establishes the limits of its applicability. The theory allows inexpensive calculation of important geophysical parameters of reservoir stimulation for given pore geometries, such as the frequency and amplitude of vibrations needed to mobilize the residual oil. The theoretical mobilizing acceleration in seismic waves for a given frequency is accurate to within approximately 30% or better when checked against CFD. The advantages of the viscous theory over the inviscid one are twofold. The former can calculate complete time histories of forced displacement of an oil blob in a pore channel, including retardation by capillary forces, mobilization by vibrations, and an ensuing Haines jump. It also provides an approximately factor-of-two improvement in the calculation of the mobilizing acceleration needed to unplug a static ganglion.

INTRODUCTION

Interest in vibrational and acoustic stimulation of oil reservoirs as a potential method of tertiary petroleum recovery has a long history (see Beresnev and Johnson, 1994, for a review; see also Nikolaevskiy et al., 1996; Roberts et al., 2001; Dobronravov, 2002; Poesio et al., 2002; Roberts et al., 2003; Roberts, 2005). However, theory and numerical simulations elucidating the underlying physics responsible for the mobilizing effect of vibrations on residual hydrocarbons were not developed until the last decade (Graham and Higdon, 2000; Hilpert et al., 2000; Iassonov and Beresnev, 2003; Beresnev et al., 2005; Li et al., 2005; Beresnev, 2006; Iassonov and Beresnev, 2008; Pride et al., 2008). Considering that one of the fundamental reasons for unrecoverable oil is the entrapment of isolated blobs in pore constrictions by capillary forces, the theoretical studies have exposed the pore-scale mechanism of vibration-induced inertial forcing pushing the stuck ganglia over their capillary barriers. We define the capillary barrier here as a resistive force that a ganglion needs to overcome to pass through a constricted opening in a porous channel.

The physics of the entrapment is generally well understood (Taber, 1969; Melrose and Brandner, 1974; Morrow, 1979; Oh and Slattery, 1979; Payatakes, 1982; Wardlaw, 1982). The existence of the capillary barrier is known as the Jamin effect (Taber, 1969). As reviewed by Iassonov and Beresnev (2008), it is caused by the inverse dependence of the capillary pressure in a pore channel on the channel's radius according to Laplace's law. As an oil blob, driven by an external pressure gradient, enters a narrow constriction, a pressure imbalance is created within the blob opposing the motion until this imbalance equates the external pressure difference across the blob, at which moment the motion stops. The oil becomes immobile unless the external forcing is increased to push it through the narrowest point in the constriction.

As detailed by Graham and Higdon (2000), Beresnev et al. (2005), and Iassonov and Beresnev (2008), the key variables controlling the "height" of the capillary barrier for an oil blob of certain length attempting to penetrate a porous constriction are the radius of the constriction, the length of the blob, and the background pressure gradient. For a population of residual ganglia in a natural reservoir, one typically encounters a continuum of capillary barriers. Applying a seismic wave with a certain frequency and amplitude provides sufficient inertial forcing to push some ganglia over their respective barriers, and the percentage of mobilized ganglia is predicted to grow with the increasing amplitude and decreasing frequency. At a given frequency, a certain amplitude must be reached that is called the threshold (the mobilization) amplitude. What is important for the mobilization is the acceleration developed by the seismic wave because it creates an inertial body force adding to the background gra-

dient. That is why, when using the term amplitude, we will imply the amplitude of acceleration.

Graham and Higdon's (2000) and Iassonov and Beresnev's (2008) studies are largely computational, whereas Beresnev (2006) formulates an inviscid dynamic theory of a ganglion's motion under the effect of vibratory excitation, based on the balance of forces acting on it. Pride (2008) reiterates the main conclusions regarding the factors controlling the ganglia mobilization. Beresnev et al. (2005) and Li et al. (2005) verify the frequency and amplitude effects on the ganglia liberation in a direct laboratory experiment; Chrysikopoulos and Vogler (2006) report further laboratory evidence of the mobilizing effect of vibrations on the residual ganglia.

A nonwetting oil blob sliding along a water film adsorbed on a pore's wall can arguably be considered frictionless. This observation was the basis for Beresnev's (2006) inviscid theory. However, if any amount of shearing occurs at the wetting-/nonwetting-phase contact line, it will create a viscous stress and contribute an additional force resisting the motion, not accounted for by an inviscid theory. Because the no-slip boundary condition still applies at the pore wall, the magnitude of the viscous stress will be a function of the thickness of the adsorbed film, which is a quantity not presently constrained by any theory. Such thicknesses have to be prescribed as a problem parameter.

A natural way to quantify the viscous stress for a two-phase fluid motion is through a model of core-annular Poiseuillean flow (e.g., Middleman, 1995, section 2-1), with different film thicknesses assumed. It will allow calculation of the parameters of the seismic field required for the mobilization of oil ganglia, such as the frequency and amplitude, with viscosity of the fluids taken into account. Such calculations can then be compared with the results of the inviscid theory, providing the magnitude of viscous effects on the parameters of seismic stimulation. The validity of the improved viscous model can be checked against generally more accurate computational fluid dynamics, which also is not part of Beresnev's (2006) study. Developing the improved viscous model of seismic stimulation, comparing it with the results of the inviscid model, and verifying the theory against computational fluid dynamics constitute the goals of the present investigation.

According to these objectives, the study proceeds as follows. We first formulate a modified version of Beresnev's (2006) equation of motion of an oil ganglion to include the viscosity effect based on the core-annular Poiseuillean flow. We then provide solutions of the equation and compare them with the solutions obtained from computational fluid dynamics, the latter serving as a reasonable, although not perfect, benchmark. This process estimates the error in computing the parameters of vibroseismic stimulation of oil production, such as the mobilizing frequency and acceleration, using the new viscous theory. We also look at the differences between the results computed from the inviscid and viscous theories, verifying the limits of applicability of the former. A synopsis of findings concludes the study.

THE GANGLION'S EQUATION OF MOTION INCLUSIVE OF VISCOUS FORCES

Consider a body of nonwetting fluid flowing in an axisymmetric, sinusoidally constricted pore channel with a constant-thickness film (with thickness dh) deposited on the channel's wall. The axial coor-

dinate is z. The radius of the fluid/fluid interface $r_i(z)$ follows the equation

$$r_i(z) = r_{max}\left[1 + \frac{1}{2}\left(\frac{r_{min}}{r_{max}} - 1\right)\left(1 + \cos \pi \frac{z}{L}\right)\right], \quad (1)$$

where $2L$ is the channel's wavelength, and r_{min} and r_{max} are the minimum and the maximum radii of the blob, respectively. Such a simplified capillary-tube model, revealing much of the physics of entrapment and mobilization, has been commonly considered before (e.g., Oh and Slattery, 1979; Wardlaw, 1982; Gauglitz and Radke, 1989; Graham and Higdon, 2000; Hilpert et al., 2000).

For a ganglion driven by a constant background pressure gradient ∇P (assuming $\nabla P \equiv \partial P/\partial z$) in the presence of externally induced vibratory inertial forcing and a resisting capillary force, in the frictionless case, Beresnev (2006, equation 8) formulates an equation of motion representing the balance of the corresponding body forces acting on the center-of-mass of the ganglion,

$$\frac{d^2(z_1/L)}{dt^2} - \frac{2\sigma}{\rho_{oil}L\ell}\left[\frac{1}{r_i(z_1)\sqrt{1 + r_i'^2(z_1)}}\right.$$
$$\left. - \frac{1}{r_i(z_1 + \ell)\sqrt{1 + r_i'^2(z_1 + \ell)}}\right] + \frac{a(t)}{L} + \frac{\nabla P}{\rho_{oil}L} = 0.$$
$$(2)$$

Here z_1/L is the dimensionless coordinate of the trailing three-phase contact line, ρ_{oil} is the density of the oil (core) phase, σ is the oil/water interfacial tension, ℓ is the length of the blob measured between the trailing and leading three-phase contact lines (see Figure 1 for an illustration), and $a(t)$ is the time-dependent acceleration of the solid wall. This acceleration provides an "inertial" driving force that, added to the background gradient, causes the blob's motion relative to the wall and its eventual mobilization (Graham and Higdon, 2000; Beresnev et al., 2005). The smallness of residual oil ganglia with respect to a seismic wavelength allows considering the inertial driving force constant over the length of the oil at any given time (Beresnev, 2006, p. N48). The "prime" symbol at r_i indicates the derivative with respect to z. The terms $r_i(z_\ell)\sqrt{1 + r_i'^2(z_1)}$ and $r_i(z_1 + \ell)$ $\sqrt{1 + r_i'^2(z_1 + \ell)}$ in equation 2 are the exact radii of the left and right menisci, respectively (Hilpert et al., 2000, equation 20).

As stated in the Introduction, if shearing at the fluid/fluid interface is present, it will introduce an additional resisting viscous force. Such a shearing can be introduced most plausibly through the model of a two-phase steady-state Poiseuillean flow in a core-annular geometry, in which oil is the core fluid and water is the surrounding annulus. If the core radius is r_c, and the oil and water viscosities are μ_{oil} and μ_w, the axial component of the Poiseuillean velocity $u(r)$ in the core obeys the equation
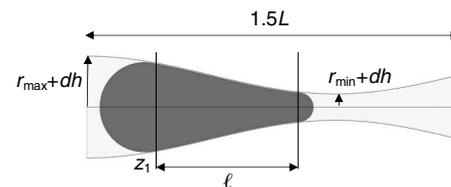

Figure 1. Initial geometry for the CFD simulations. The channel's full wavelength is $2L$.

$$u(r) = -\frac{\nabla P}{4\mu_{\text{oil}}}(r_c^2 - r^2) - \frac{\nabla P}{4\mu_w}[(r_c + dh)^2 - r_c^2] \quad (3)$$

([Middleman, 1995](#), equation 2-1.9). The shear stress at the fluid/fluid interface is then, by definition, calculated as

$$\tau|_{r=r_c} = \mu_{\text{oil}} \left.\frac{du}{dr}\right|_{r=r_c} = \frac{r_c \nabla P}{2}, \quad (4)$$

where the derivative has been found from equation 3.

According to our conceptual model of the oil body sliding along the viscous film, this shear stress, then equivalent to a friction force, is expected to be controlled by the speed of the motion of the ganglion dz_1/dt, which we equate with the Poiseuillean velocity in the center of the channel, $r = 0$. Writing equation 3 for $r = 0$, solving it for ∇P, and substituting the result into equation 4 with $u(0) \equiv dz_1/dt$ then leads to the shear stress in the form

$$\tau|_{r=r_c} = -\frac{2\mu_{\text{oil}}}{r_c\left[1 + \dfrac{\mu_{\text{oil}}}{\mu_w}\dfrac{dh}{r_c}\left(2 + \dfrac{dh}{r_c}\right)\right]}\frac{dz_1}{dt}, \quad (5)$$

which expresses it through the ganglion's speed.

Because equation of motion 2 is written through body forces, the shear stress (equation 5) should be converted to a body force as well. This stress is the viscous force per unit area acting on the surface of the cylinder with radius r_c and length ℓ; multiplying this stress by the total area of the cylinder and dividing by its volume, we obtain the frictional body force as equation 5 multiplied by $2/r_c$.

A straight cylindrical core-annular flow has been assumed so far in the derivation of the viscous body force. The actual ganglion shape follows an axisymmetric equation 1, in which the radius varies from r_{min} to r_{max}. As the best approximation, we substitute the average of $\overline{r_c} \equiv (r_{\text{min}} + r_{\text{max}})/2$ for r_c in the final equation. Normalizing the frictional body force by $\rho_{\text{oil}}L$ as was done in equation 2, we then obtain the expression

viscous-body-force

$$= -\frac{4\mu_{\text{oil}}}{\rho_{\text{oil}}\overline{r_c}^2\left[1 + \dfrac{\mu_{\text{oil}}}{\mu_w}\dfrac{dh}{\overline{r_c}}\left(2 + \dfrac{dh}{\overline{r_c}}\right)\right]}\frac{d(z_1/L)}{dt}. \quad (6)$$

This term should be added, with a positive sign, to the left-hand side of equation 2, which becomes the modified equation of motion of the ganglion that takes into account the viscous resistance. From now on, we will call the result the viscous equation, and it will be the subject of the subsequent analysis.

Our application of the model of Poiseuillean core-annular flow in a straight cylindrical channel to a channel with varying wall profile is valid in the "small-slope" ("lubrication") approximation ([Panton, 1996](#), figure 21.3). For the channels with sinusoidal geometry, the approximation applies if the slope parameter α, equal to the ratio of the maximum radius of the tube to its half wavelength, is kept smaller than one ([Gauglitz and Radke, 1990](#), figure 2; [Beresnev and Deng, 2010](#)). This is the restriction on the geometry that we must follow in the examples below.

VIBRATORY MOBILIZATION OF RESIDUAL OIL WITH VISCOSITY TAKEN INTO ACCOUNT

Comparison of the viscous model with computational fluid dynamics

Methodology of comparison

Equation 2, with the friction term added, is a new viscous model that describes the dynamics of the oil ganglion. Its solutions provide a complete time history of the blob's displacement. For practical purposes, however, it is important to verify if this equation provides an accurate prediction of the parameters of vibroseismic stimulation, such as the amplitude and frequency of vibrations that mobilize a given stuck body of oil. Our validation will be based on computational fluid dynamics (CFD), which we assume can provide a generally accurate solution of the hydrodynamic problem underlying the geophysical one at hand. The vibroseismic parameters are first obtained from the numerical solution of the viscous equation. Then the same geometric scenario is run in a fully hydrodynamic CFD simulation, and the parameters are compared.

Our CFD simulations have been performed using the commercial code Fluent (manufactured by ANSYS, Inc.), which incorporates the finite-volume discretization scheme to solve the full system of equations of fluid mechanics for the two-phase flow on a spatial grid. An example of an initial geometry of a ganglion entrapped in a pore constriction, used as a starting configuration in CFD, is shown in Figure 1. All simulations were performed on a mesh of quadrilateral cells; mesh-refinement studies were carried out to ensure that the solutions were grid independent.

As detailed by [Beresnev et al. (2005)](#), [Beresnev (2006)](#), and [Iassonov and Beresnev (2008)](#), as the frequency of vibrations increases, so generally does the amplitude needed to unplug the blob. For every mobilization frequency, therefore, runs with several amplitudes are required to bracket, by trial and error, the threshold amplitude at which the mobilization takes place. The CFD simulations are computationally extremely intensive. It should be remembered also that typically as many as several periods of vibratory drive are needed to push the ganglion completely through the constriction ([Beresnev, 2006](#)). The CFD simulations thus have to proceed for a time span of several periods. The computer time required for this imposes practical limitations on the lowest frequency (longest period) that we could use.

For example, computing one scenario from the initial entrapped configuration to the liberation moment, with the necessary stability and convergence constraints, requires two to three weeks of CPU time on a modern four-processor workstation for the seismic frequency of 50 Hz. Considering that several such runs are needed to bracket the mobilizing acceleration, the total computer time to resolve the unplugging acceleration at 50 Hz is about three months. For this reason, 50 Hz was the lowest frequency used. The computer time restriction is much more relaxed as one moves upward in the frequency. This explains the relatively high-frequency range of our comparisons.

Similar restrictions apply to the size of the computational domain (the pore size) (Figure 1). To ensure the reliability of CFD simulations, the absolute size of grid cells has to stay about the same no matter how large the domain is. This practically means that the computing time necessarily increases beyond plausible limits if too large a channel is simulated. In the following, we show results for two

channel geometries: $r_{min} = 10^{-5}$ m, $r_{max} = 2 \times 10^{-5}$ m (we will call it the case of low aspect ratio) and $r_{min} = 10^{-5}$ m, $r_{max} = 4 \times 10^{-5}$ m (the case of high aspect ratio), L and ℓ being 10^{-4} m and $0.6 \times L$, respectively. This was achieved as a compromise between satisfying computational limitations and staying within realistic pore sizes for a natural oil reservoir. The slope parameter α is kept under one ($\alpha = 0.2$ and 0.4, respectively). Because the channel geometry (through the resisting capillary force) dictates the total external forcing required for the mobilization, this forcing (the static gradient plus vibratory acceleration) for the geometries chosen was necessarily constrained to be relatively large as well. However, it should be remembered that absolute values of the vibratory acceleration and background gradient ∇P are scaled up and down by the pore geometry and the ganglion size (Beresnev, 2006) and should not be viewed as having any particular meaning.

The total number of quadrilateral cells for the geometries used ranged from 23,216 to 83,450. The fluid parameters were as follows: $\sigma = 0.04$ N/m, $\mu_{oil} = 0.01$ Pa s, $\mu_w = 0.001$ Pa s. The densities of oil and water were taken equal to 1000 kg/m^3. Figures 2 and 3 show the results of comparisons of the viscous model against CFD for the low- and high-aspect-ratio pores, respectively. On the graphs on the left-hand side, one point represents, for the geometry values listed in figure captions, the values of the acceleration amplitude versus frequency. These acceleration amplitudes are required to mobilize an entrapped ganglion. The constant background gradients are indicated also in the captions; by definition of the entrapment condition, they are insufficient to mobilize the ganglion without the vibrations applied. Graphs are plotted separately for the CFD (squares) and viscous-model (circles) results in the frequency range of 50 to 1000 Hz.
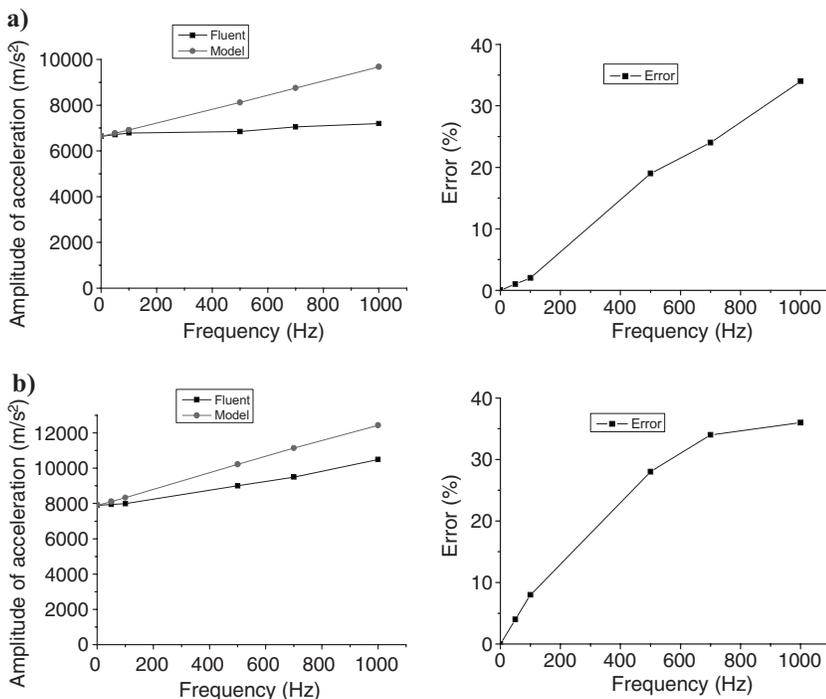
As noted, the absolute magnitudes of acceleration are high; however, these are constrained by the geometry choices and merely serve to compare the values from CFD and the model. The relative error in the threshold acceleration amplitude, plotted on the right in Figures 2 and 3, is calculated as the difference between the CFD and viscous-model values normalized by the CFD value. In addition, Figure 2 shows results for two film thicknesses, $dh = 0.1 \times r_{min}$ (Figure 2a) and $dh = 0.05 \times r_{min}$ (Figure 2b).

In CFD simulations, we maintained a constant pressure difference between the left and right boundaries of the computational domain (see Figure 1), corresponding to the postulated pressure gradient. However, the CFD approach is free from simplifying assumptions made in the derivation of the theoretical model that had made the theory tractable. For example, the local pressure gradient in a two-phase flow, such as shown in Figure 1, with the menisci present, is neither constant nor steady, nor is the length of the moving blob (the theoretical model assumes both ∇P and ℓ to be constant). This shows that care needs to be exercised in determining how to judiciously define the equivalence between the initial configurations in CFD and the analytic model, considering the fundamental differences between their levels of approximation of reality.

We define the equivalence as follows. We set the same initial length of the ganglion ℓ; however, in CFD it will vary as the ganglion leaves its entrapped configuration. Next we assign the same "global" ∇P. In the CFD simulation, it is formally introduced by dividing the pressure difference across the domain by the domain length. Finally, we enforce that the initial configurations in CFD and the model have the same static mobilization threshold. This is reflected in the fact that the curves in Figures 2 and 3 (left) converge at zero frequency.

The equality of the static thresholds means that, in the initial entrapped configuration without vibrations applied, the ganglion will become mobilized in both the model and CFD by adding the same additional constant body force (a step jump) to the existing background gradient. Because this is a constant jump, we conveniently call it zero frequency. To be plotted on the same scale in Figures 2 and 3, this step increase in the body force is converted to units of acceleration by dividing it by the fluid density. To ensure the equality of the static thresholds, the ∇P in the model and CFD have to be slightly adjusted; however, this equality is physically more meaningful than that of the formally defined "global" gradients. Following this procedure does not generally lead to the same static mobilization thresholds for different film thicknesses, which is exemplified by Figure 2a and b (left panels).

Figure 2. Comparison of CFD simulations and viscous model: $r_{max} = 2 \times 10^{-5}$ m, $r_{min} = 10^{-5}$ m (a) $dh = 0.1 \times r_{min}$, $|\nabla P| = 3.98 \times 10^7$ N/m^3; (b) $dh = 0.05 \times r_{min}$, $|\nabla P| = 3.66 \times 10^7$ N/m^3.

Summary of geophysical results

With the "static" equivalence of the initial conditions defined, we can make comparisons of the mobilizing effect of vibrations at frequencies not equal to zero. Figure 2 shows that the results obtained from CFD and the viscous model (constrained to be the same at zero frequency) start to diverge as the frequency increases to 1000 Hz. This is to be expected because oscillatory forcing

of a realistic fluid is associated with complex flow patterns, which are adequately captured by the computational fluid dynamics but not by the model equation; the ability of the theory to represent realistic dynamic behavior can therefore be predicted to degrade with the frequency. However, as the comparison shows, the simple model equation still provides a correct order-of-magnitude prediction of the vibroseismic-mobilization parameters, relative to CFD, even at frequencies as high as 1000 Hz.

As the right panel in Figure 2 indicates (the case of the low aspect ratio), the maximum error grows to 34% and 18% at 1000 Hz for the two film thicknesses ($dh = 0.1 \times r_{min}$ and $0.05 \times r_{min}$, respectively). The behavior of the curves for the aspect ratio that is twice as large (Figure 3, left) ($dh = 0.1 \times r_{min}$) does not follow this simple pattern, however. The error (Figure 3, right) is smaller, has an opposite sign, and seems to peak at 14% at the lowest frequency of 50 Hz instead of the highest frequency. It is difficult to explain fully these quantitative differences, which might have to do with the increased slope of the wall of the channel, other than noting that the comparisons indicate that the maximum error in the determination of the parameters of vibroseismic stimulation from the viscous model, relative to CFD, is expected to be on the order of tens of percent.

An approximately linear increase in the amplitude of unplugging acceleration with increasing frequency is seen in Figures 2 and 3 (left panels). This result is to be expected and was explained on physical grounds by Iassonov and Beresnev (2008, p. 468 and figure 7a).

Comparison of the viscous and inviscid models

When mobilizing external forcing is applied to a nonwetting ganglion stuck in a constriction, the ganglion moves slowly, overcoming resistance, until its leading meniscus reaches the neck of the constriction; past that point, the ganglion is liberated and precipitously jumps out. The latter is known as the Haines jump, broadly defined here as an impulsive motion of the meniscus as it retreats from the constriction (e.g., Melrose and Brandner, 1974, figure 2; Gauglitz and Radke, 1989, figure 2). In the stage before it, the capillary force is the principal force resisting the motion. It progressively increases as the ganglion moves into the constriction and at every instance balances the forces that push the ganglion forward (the background gradient and vibratory inertial forcing). This is the key to understanding the entrapment phenomenon: viscous forces are not needed to immobilize the oil. The motion before liberation is always restricted by capillarity and can be, in principle, calculated without accounting for the viscosity.

A totally different pattern emerges past the liberation point, as the leading meniscus leaves the neck of the constriction. The resisting capillary force instantaneously vanishes, and in the absence of such, the ganglion accelerates infinitely. In other words, the Haines jump goes to infinity (Beresnev, 2006, figures 3 and 5). This rationale explains why the inviscid model can predict the condition for the mobilization but not the motion of the blob after it has been "unplugged." We now wish to check if the incorporation of a viscosity term leads to a finite jump and continuity in the entire time history of the motion.

Figure 4 presents, as an example, the solutions of the inviscid equation 2 (left) and the viscous equation (right), showing the time history of the

bubble displacement z_1/L from its entrapped configuration after the vibrations with frequency of 1000 Hz have been turned on at $t = 0$ s. The geometry is indicated in the figure caption. The difference between the displacement behaviors is as has been anticipated. The bubble becomes liberated in a fraction of the vibration period in both cases; the liberation moment is only slightly delayed by the friction in the viscous case (the mobilization moments are indicated by arrows). However, the subsequent motion in the inviscid case constitutes an infinite Haines jump. A progressive motion through a series of constricted pores can be tracked only in the viscous model. Having experienced the first Haines jump, the blob reaches the next constriction, experiences two back-and-forth movements under the effect of the vibratory forcing, corresponding to two periods of vibration, then becomes mobilized during the third period, experiences the next Haines jump, and the pattern is repeated as the ganglion makes its way through the series of constrictions (Figure 4, right).

The Haines jumps (the steepest segments of the trajectory) are indicated also by arrows in Figure 4, right. They are, of course, much subdued by the viscous resistance, but their trajectory is still visibly steeper than the trajectory at any other part of the time history. The number of periods of the blob's oscillations in the subsequent entrapped positions before the following Haines jumps can be variable, as it is dictated by a pattern of interference between forced and free oscillations (Beresnev, 2006, p. N51). In this example, it is equal to two. The entire time history calculated with the viscosity accounted for has a realistic periodic character, showing all principal phases of motion expected from the balance of governing forces. However, the fact of the ganglion mobilization is predicted correctly by the inviscid theory.

It would be important also for the geophysical applications to compare the change in the minimum (threshold) mobilizing acceleration calculated from the inviscid and viscous theories. It can be expected that, all conditions being equal, adding viscosity to the model will increase, through the added resistive force, the threshold value of acceleration needed to liberate a ganglion from its entrapped configuration. As an example, calculations show that at seismic frequencies of 20 and 50 Hz and the geometry and ∇P as in Figure 4, the ratios of the "viscous" to "inviscid" threshold accelerations are both equal to 2.1. The acceleration needed to mobilize a stuck blob indeed increases with added viscosity as anticipated. This ratio also quantifies the magnitude of the effect that the new viscous theory has on the prediction of unplugging acceleration, which is finite but not overwhelming.
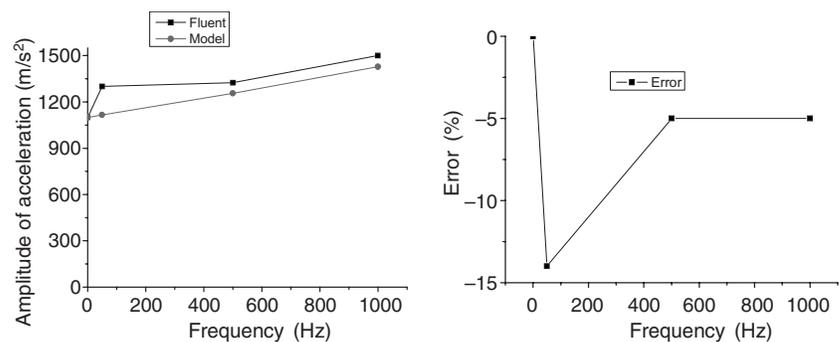

Figure 3. Comparison of CFD simulations and viscous model: $r_{max} = 4 \times 10^{-5}$ m, $r_{min} = 10^{-5}$ m, $dh = 0.1 \times r_{min}$, $|\nabla P| = 9.01 \times 10^7$ N/m³.

DISCUSSION

We have developed a model describing the motion of a nonwetting oil ganglion driven through a constricted pore under the effect of an imposed pressure gradient and external vibrations and resisted by capillary force and viscous friction. The incorporation of viscous stress has been achieved through a Poiseuillean core-annular flow formulation. The earlier model of Beresnev (2006) assumed the capillary force as the only one resisting the motion, which provided a realistic description of the forced oscillations up to the mobilization moment but could not track the entire trajectory of the ganglion as it moved through a succession of pores. The primary goal of this theoretical development is to provide an improved quantitative description of seismic mobilization of residual oil as a tool in enhanced oil recovery (Roberts et al., 2003).

In following the traditional approach of reducing the complex porous media to their most basic elements — single capillary channels — the theoretical model used is one of a constricted capillary tube. This simplification allowed many investigators to make the analysis tractable and reveal the basic physics of the entrapment and mobilization of the residual oil; the same approach can be applied to the seismic-stimulation phenomenon. As emphasized by Iassonov and Beresnev (2008, p. 472), the approach does not take into account the pore interconnectivity and the presence of multiple menisci.

Experimental evidence already suggests that calculations, based on the proposed ganglion-liberation mechanism, can be successfully applied to explaining the seismic-mobilization parameters observed in a laboratory system of interconnected pores (Beresnev et al., 2005; Li et al., 2005). An oil ganglion extending down gradient and having multiple lateral branches is, of course, a more complex system than a blob in a constricted tube. It is nonetheless reasonable to assume that the principal motion will still proceed along the direction of the external gradient, and the mobilization will occur through the menisci residing closest to their mobilization thresholds, to which calculations of the single-tube theory can be applied. The theory thus is expected to provide the basic physical understanding of the mobilization process at a single-pore level even in the case of more complex, two- and three-dimensional pore systems.

In addition, the theory presented does not consider a possibility of the continuous core phase breaking up into beads in pore constrictions when the ganglion protrudes far enough through the narrowest point, that is, beyond the seismic mobilization stage (Roof, 1970; Tsai and Miksis, 1994; Chrysikopoulos and Vogler, 2006). In this context, the model discussed should be viewed as providing a theoretical description of the ganglion's seismic mobilization and its motion through the constriction until the conditions for the initiation of the breakup have been met. A smaller ganglion will arise after that.
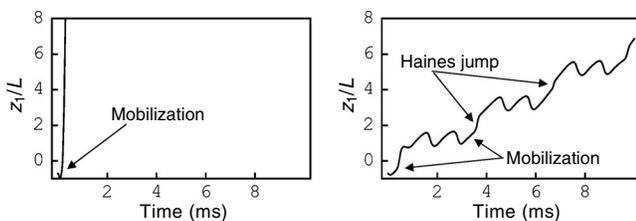

Figure 4. Axial position of the ganglion under the effect of vibrations calculated from the inviscid (left) and viscous (right) models: $r_{max} = 2 \times 10^{-5}$ m, $r_{min} = 10^{-5}$ m, $dh = 0.05 \times r_{min}$, $|\nabla P| = 3.66 \times 10^7$ N/m^3, $f = 10^3$ Hz.

The improved viscous stimulation model has been checked against a finite-volume CFD code. Of principal interest is the correctness of estimation of the important parameters of vibroseismic petroleum recovery, such as the frequency and amplitude, calculated from the viscous theory, relative to CFD. Using the model equation for such calculations for plausible practical applications has significant advantages. At seismic frequencies, computational fluid dynamics is prohibitively expensive. For example, at 50 Hz, it takes as many as three months of CPU time on a present-day multiprocessor workstation to compute a threshold mobilizing acceleration that a seismic source needs to develop. Using the model equation, this takes only several seconds.

CONCLUSIONS

Comparison of the seismic solutions between CFD and the viscous equation, carried out in the frequency range of 50 to 1000 Hz, shows that the simple dynamic model predicts the minimum acceleration required to mobilize a static ganglion at a given vibration frequency with an error of about 30% or smaller, relative to CFD. The error might depend on the geometry and the frequency. Assuming CFD as a reliable benchmark, this can be considered a practically satisfactory accuracy of the model, considering its simplicity and the ease of obtaining its numerical solutions. The viscous equation provides complete time histories of a ganglion's displacement through a porous channel, indicating all principal stages of motion, such as the retardation by restraining capillary force, mobilization due to the cumulative effect of vibrations and background static forcing, a Haines jump again followed by retardation, and so on.

Taking viscosity into account necessarily increases the magnitude of the vibratory force required for the mobilization, due to an increased resistance to flow. At seismic frequencies of 20 and 50 Hz, for example, the threshold mobilizing accelerations are increased by approximately a factor of two in the viscous case for the geometries analyzed, relative to the inviscid model. This quantifies the gain in accuracy of estimating the practical field parameters of vibroseismic stimulation achieved by using the viscous equation of motion.

The viscous force depends on the assumed thickness of the wetting film adsorbed on pore walls. In the absence of a constraining theory, this thickness value has to be prescribed and should be considered one of the model's parameters.

The proposed model provides an improved quantitative tool that can be used in the estimation of the parameters of vibroseismic reservoir stimulation. Whether the required elastic-wave amplitudes can be achieved realistically with the existing borehole acoustic sources is a separate question.

In summary, the viscous analytic model of oil-ganglion dynamics proves to be a convenient, inexpensive, and reasonably accurate tool for calculating practical parameters of seismic stimulation of residual oil for prescribed pore geometries.

ACKNOWLEDGMENTS

REFERENCES

Beresnev, I. A., 2006, Theory of vibratory mobilization of nonwetting fluids entrapped in pore constrictions: Geophysics, **71**, no. 6, N47-N56.

Beresnev, I. A., and W. Deng, 2010, Theory of breakup of core fluids surrounded by a wetting annulus in sinusoidally constricted capillary channels: Physics of Fluids, **22**, 012105-1–012105-10.

Beresnev, I. A., and P. A. Johnson, 1994, Elastic-wave stimulation of oil production: A review of methods and results: Geophysics, **59**, 1000–1017.

Beresnev, I. A., R. D. Vigil, W. Li, W. D. Pennington, R. M. Turpening, P. P. Iassonov, and R. P. Ewing, 2005, Elastic waves push organic fluids from reservoir rock: Geophysical Research Letters, **32**, L13303.

Chrysikopoulos, C. V., and E. T. Vogler, 2006, Acoustically enhanced ganglia dissolution and mobilization in a monolayer of glass beads: Transport in Porous Media, **64**, 103–121.

Dobronravov, O. V., 2002, A new technology of reservoir stimulation through exposure to weak seismic waves: First Break, **20**, 376–382.

Gauglitz, P. A., and C. J. Radke, 1989, Dynamics of Haines jumps for compressible bubbles in constricted capillaries: American Institute of Chemical Engineers Journal, **35**, 230–240.

———, 1990, The dynamics of liquid film breakup in constricted cylindrical capillaries: Journal of Colloid and Interface Science, **134**, 14–40.

Graham, D. R., and J. J. L. Higdon, 2000, Oscillatory flow of droplets in capillary tubes: Part 2 — Constricted tubes: Journal of Fluid Mechanics, **425**, 55–77.

Hilpert, M., G. H. Jirka, and E. J. Plate, 2000, Capillarity-induced resonance of oil blobs in capillary tubes and porous media: Geophysics, **65**, 874–883.

Iassonov, P. P., and I. A. Beresnev, 2003, A model for enhanced fluid percolation in porous media by application of low-frequency elastic waves: Journal of Geophysical Research, **108**, ESE2–1-ESE2–9.

———, 2008, Mobilization of entrapped organic fluids by elastic waves and vibrations: SPE Journal, **13**, 465–473.

Li, W., R. D. Vigil, I. A. Beresnev, P. P. Iassonov, and R. P. Ewing, 2005, Vibration-induced mobilization of trapped oil ganglia in porous media: Experimental validation of a capillary-physics mechanism: Journal of Colloid and Interface Science, **289**, 193–199.

Melrose, J. C., and C. F. Brandner, 1974, Role of capillary forces in determining microscopic displacement efficiency for oil recovery by waterflooding: Journal of Canadian Petroleum Technology, **13**, 54–62.

Middleman, S., 1995, Modeling axisymmetric flows: Academic Press.

Morrow, N. R., 1979, Interplay of capillary, viscous and buoyancy forces in the mobilization of residual oil: Journal of Canadian Petroleum Technology, **18**, 35–46.

Nikolaevskiy, V. N., G. P. Lopukhov, Y. Liao, and M. J. Economides, 1996, Residual oil reservoir recovery with seismic vibrations: SPE Production and Facilities, **11**, 89–94.

Oh, S. G., and J. C. Slattery, 1979, Interfacial tension required for significant displacement of residual oil: SPE Journal, **19**, 83–96.

Panton, R. L., 1996, Incompressible flow, 2nd edition: John Wiley and Sons.

Payatakes, A. C., 1982, Dynamics of oil ganglia during immiscible displacement in water-wet porous media: Annual Review of Fluid Mechanics, **14**, 365–393.

Poesio, P., G. Ooms, S. Barake, and F. van der Bas, 2002, An investigation of the influence of acoustic waves on the liquid flow through a porous material: Journal of the Acoustical Society of America, **111**, 2019–2025.

Pride, S. R., E. G. Flekkøy, and O. Aursjø, 2008, Seismic stimulation for enhanced oil recovery: Geophysics, **73**, no. 5, O23–O35.

Roberts, P. M., 2005, Laboratory observations of altered porous fluid flow behavior in Berea sandstone induced by low-frequency dynamic stress simulation: Acoustical Physics, Supplement **1**, S140–S148.

Roberts, P. M., I. B. Esipov, and E. L. Majer, 2003, Elastic wave stimulation of oil reservoirs: Promising EOR technology? The Leading Edge, **22**, 448–453.

Roberts, P. M., A. Sharma, V. Uddameri, M. Monagle, D. E. Dale, and L. K. Steck, 2001, Enhanced DNAPL transport in a sand core during dynamic stress stimulation: Environmental Engineering Science, **18**, 67–79.

Roof, J. G., 1970, Snap-off of oil droplets in water-wet pores: SPE Journal, **10**, 85–90.

Taber, J. J., 1969, Dynamic and static forces required to remove a discontinuous oil phase from porous media containing both oil and water: SPE Journal, **9**, 3–12.

Tsai, T. M., and M. J. Miksis, 1994, Dynamics of a drop in a constricted capillary tube: Journal of Fluid Mechanics, **274**, 197–217.

Wardlaw, N. C., 1982, The effects of geometry, wettability, viscosity and interfacial tension on trapping in single pore-throat pairs: Journal of Canadian Petroleum Technology, **21**, 21–27.